





Glueballs at physical pion mass*

Feiyu Chen (陈飞宇)^{1,2†}  Xiangyu Jiang (蒋翔宇)^{1,2}  Ying Chen (陈莹)^{1,2}  Keh-Fei Liu (刘克非)³
Wei Sun (孙伟)¹  Yi-Bo Yang (杨一玻)^{2,4,5,6} 

¹Institute of High Energy Physics, Chinese Academy of Sciences, Beijing 100049, China

²School of Physics Sciences, University of Chinese Academy of Sciences, Beijing 100049, China

³Department of Physics and Astronomy, University of Kentucky, Lexington, Kentucky 40506, USA

⁴CAS Key Laboratory of Theoretical Physics, Institute of Theoretical Physics, Chinese Academy of Sciences, Beijing 100190, China

⁵School of Fundamental Physics and Mathematical Sciences, Hangzhou Institute for Advanced Study, UCAS, Hangzhou 310024, China

⁶International Centre for Theoretical Physics Asia-Pacific, Beijing/Hangzhou, China

Abstract: Glueballs are investigated through gluonic operators on two $N_f = 2 + 1$ RBC/UKQCD gauge ensembles at the physical pion mass. The statistical errors of glueball correlation functions are considerably reduced through the cluster decomposition error reduction (CDER) method. The Bethe-Salpeter wave functions are obtained for the scalar, tensor, and pseudoscalar glueballs by using spatially extended glueball operators defined through the gauge potential $A_\mu(x)$ in the Coulomb gauge. These wave functions exhibit similar features of non-relativistic two-gluon systems and are used to optimize the signals of the related correlation functions at the early time regions, where the ground state masses are extracted. These masses are close to those from the quenched approximation and indicate the possible existence of glueballs at the physical point. The resonance feature of glueballs and the mixing with conventional mesons and multi-hadron systems should be considered in a more systematic lattice study.

Keywords: glueball, lattice QCD, exotic hadron state

DOI: 10.1088/1674-1137/accc1c

I. INTRODUCTION

In quantum chromodynamics (QCD), gluons carry color charges and have a direct strong interaction among themselves. Therefore, it is expected that hadrons can be made up of gluons solely, namely glueballs. The property of glueballs has been one of the most prominent topics in hadron physics for several decades and has been the focus of extensive and intensive experimental and theoretical studies. However, their existence has not yet been confirmed.

Glueballs are well defined objects in the quenched approximation where the quark-gluon transitions are switched off, and in quenched lattice QCD (QLQCD) studies, the existence of pure gauge glueballs has been confirmed, and their spectrum has been predicted [1, 2]. In the presence of dynamical quarks, the situation is more complicated owing to the decays of glueballs and the possible mixing between glueballs and $q\bar{q}$ mesons. There

have been a few preliminary full-QCD lattice studies [3–5] at pion masses much larger than the physical value, in which possible glueball states with masses close to the predictions from QLQCD were observed. However, it is still challenging to verify the previous glueball studies at the physical pion mass because of the computational cost, as glueball related lattice studies usually require large statistics of thousands of gauge configurations, which is computationally prohibitive for physical pion masses and large spatial volumes at the present stage. Fortunately, the cluster decomposition principle ensures that the correlation length between the glueball operators is insensitive to the volume and can be implemented to reduce the statistical errors of glueball correlation functions. In Refs. [6–8], a cluster decomposition error reduction (CDER) method was introduced to suppress the statistics requirement on lattices with large spatial volumes. In this work, we use the CDER method to trade the statistical uncertainty for a negligible systematic one and obtain the clear

Received 6 March 2023; Accepted 12 April 2023; Published online 13 April 2023

* Supported by the Strategic Priority Research Program of Chinese Academy of Sciences (XDB34030300, XDPB15), the National Key Research and Development Program of China (2020YFA0406400), and the National Natural Science Foundation of China (NNSFC) under Grants (11935017, 12070131001) (CRC 110 by DFG and NNSFC). The computations were performed on the CAS ORISE computing environment, the HPC clusters at Institute of High Energy Physics (Beijing), the China Spallation Neutron Source (Dongguan), and the Institute of Theoretical Physics. Y. Yang is also supported in part by a NSFC-DFG joint grant (12061131006 and SCHA 458/22)

† E-mail: chenfy@ihep.ac.cn



Content from this work may be used under the terms of the Creative Commons Attribution 3.0 licence. Any further distribution of this work must maintain attribution to the author(s) and the title of the work, journal citation and DOI. Article funded by SCOAP³ and published under licence by Chinese Physical Society and the Institute of High Energy Physics of the Chinese Academy of Sciences and the Institute of Modern Physics of the Chinese Academy of Sciences and IOP Publishing Ltd

mass spectrum and Bethe-Salpeter wave function with the pure glueball operators on only ~ 300 configurations at the physical pion mass.

II. NUMERICAL DETAILS

We choose two RBC/UKQCD gauge ensembles (labeled as 48I and 64I) with a $2+1$ flavor domain wall fermion at physical pion and kaon masses and with spatial sizes around 5.5 fm. The parameters of the ensembles are shown in Table 1 of Ref. [9]. To extract glueball states, we adopt the strategy used in Ref. [1, 2] to build the glueball operator set $\mathcal{S}(R^{PC}) = \{O_\alpha, \alpha = 1, 2, \dots, 24\}$ for the scalar ($R^{PC} = A_1^{++}$), pseudoscalar (A_1^{-+}), and tensor ($E^{++} \oplus T_2^{++}$) channels, where $R = A_1, E, T_2$ are the irreducible representations (irrep) of the lattice symmetry group O , and P and C are the parity and the charge conjugate quantum numbers, respectively.

Table 1. Parameters of the 48I and 64I ensembles [9].

$L^3 \times T$	a^{-1} /GeV	m_π /MeV	La /fm	N_{conf}
$48^3 \times 96$	1.730(4)	139.2(4)	5.476(12)	364
$64^3 \times 128$	2.359(7)	139.2(5)	5.354(16)	300

A. Cluster decomposition error reduction method (CDER)

It is well known that the glueball relevant lattice study usually requires large statistics, but we have only $N_{\text{conf}} \sim 300$ configurations available for the two ensembles. Fortunately, their large lattice sizes make the cluster decomposition error reduction method (CDER) [7] feasible for improving the signal-to-noise ratio in the calculation. The idea of CDER is as follows: because $C_{\alpha\beta}(\mathbf{r}, t) \equiv \langle 0|O_\alpha(\mathbf{r}, t)O_\beta(\mathbf{0}, 0)|0\rangle$ behaves as

$$C_{\alpha\beta}(\mathbf{r}, t) \sim \xi^{-\frac{3}{2}} e^{-m\xi} \quad (\xi \rightarrow \infty), \quad (1)$$

where m represents the lowest mass in this channel and $\xi = (\mathbf{r}^2 + t^2)^{1/2}$ represents the Euclidean separation between the sink and the source operator, the signals of $C_{\alpha\beta}$ will be undermined by statistical noise when $|\mathbf{r}|$ is beyond some length scale $|\mathbf{r}_c| \propto 1/m$. Therefore, the correlation matrix $C_{\alpha\beta}$ with the operator set $\mathcal{S}(R^{PC})$ for a given R^{PC} channel can be calculated as

$$\begin{aligned} C_{\alpha\beta}(t) &= \frac{1}{T} \sum_{\tau, \mathbf{x}, \mathbf{r}} \langle 0|O_\alpha(\mathbf{x} + \mathbf{r}, t + \tau)O_\beta(\mathbf{x}, \tau)|0\rangle \\ &\simeq \sum_{|\mathbf{r}| < r_c} K_{\alpha\beta}(\mathbf{r}, t) \equiv C_{\alpha\beta}(r_c, t), \end{aligned} \quad (2)$$

where the average over time slices is taken into account

to improve the statistics, and the kernel functions $K_{\alpha\beta}(\mathbf{r}, t)$ are introduced as

$$K_{\alpha\beta}(\mathbf{r}, t) = \sum_{\mathbf{k}} e^{-i\mathbf{k}\cdot\mathbf{r}} \langle 0|\hat{O}_\alpha(-\mathbf{k}, t)\hat{O}_\beta(\mathbf{k}, t)|0\rangle \quad (3)$$

in terms of the Fourier transformed operators $\hat{O}_\alpha(-\mathbf{k}, t) = \sum_{\mathbf{x}} e^{-i\mathbf{k}\cdot\mathbf{x}} O_\alpha(\mathbf{x}, t)$. The cutting scale parameter r_c is chosen empirically when the value of $C_{\alpha\beta}(r_c, t)$ is saturated. Note that the vacuum subtraction is necessary for A_1^{++} operators because they have the same quantum numbers as the vacuum. Before the CDER scheme is applied, for each of the A_1^{++} operators, the vacuum subtraction is performed through the replacement

$$O_\alpha(x) \rightarrow O_\alpha(x) - \frac{1}{V} \langle \sum_x O_\alpha(x) \rangle, \quad (4)$$

where V represents the 4-D volume, and $\langle O_\alpha \rangle$ is the average of O over the gauge ensemble involved. After the CDER scheme, the vacuum subtraction is successfully fulfilled. In practice, the above procedure is applied to all the considered channels.

The efficacy of CDER is illustrated in Figs. 1 and 2, where a typical $C_{\alpha\beta}(r_c, t)$ in the A_1^{++} channel at different fixed time slices is plotted versus r_c/a . One can see the central values of $C_{\alpha\beta}(r_c, t)$ at different t are saturated uniformly beyond $r_c/a = 7$, but the errors grow with an increase in r_c . In the practical calculation, we choose $r_c/a = 7$ for all the $C_{\alpha\beta}(R, t)$ in all the channels.

In each R^{PC} channel, after the correlation matrix $C_{\alpha\beta}(t)$ is estimated through Eq. (2), we perform the stand-

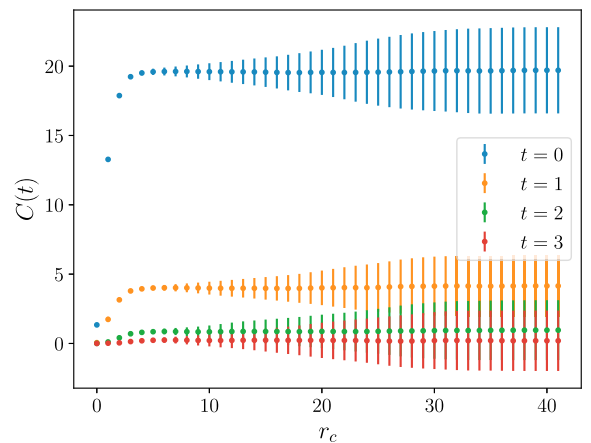


Fig. 1. (color online) Plot of the A_1^{++} correlation function at the first 4 times slices against the cutoff on the $48^3 \times 96$ lattice. The r_c is in lattice unit. As expected, the signal reaches the maximum at $r_c \sim 7a$, and only the noise increases afterwards. Here, the error bars indicate the standard deviations instead of statistical errors.

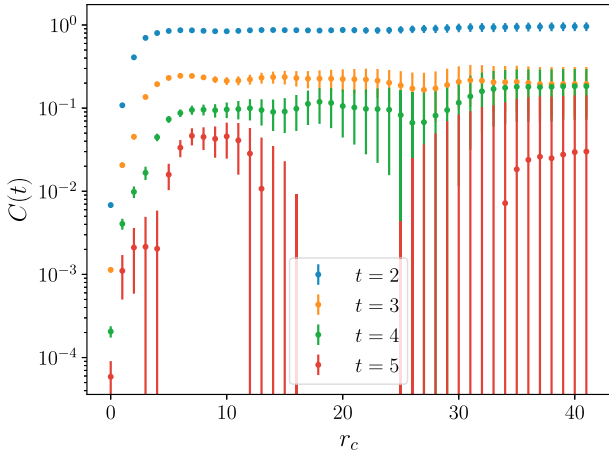


Fig. 2. (color online) Same as Fig. 1 but in logarithm scale with the standard error for larger t . One can see that the error becomes unacceptable for $r_c > 12a$. We expect that reliable results can be extracted from $r_c = 7a$.

ard variational method by solving the generalized eigenvalue problem $C_{\alpha\beta}(t)v_\beta = \lambda(t, t_0)C_{\alpha\beta}(t_0)v_\beta$. In practice, we use $t_0 = 0$ and $t = a$. The eigenvector $v_\alpha^{(n)}$ of the n -th largest eigenvalue gives an optimized operator $O_n = v_\alpha^{(n)}O_\alpha$ that is expected to couple most to the n -th lowest state $|n\rangle$. In other words, the correlation function $C_n(t)$ of O_n behaves as

$$C_n(t) = \langle 0|O_n(t)O_n(0)|0\rangle \sim e^{-m_n t}, \quad (5)$$

where the eigenvectors $v_\alpha^{(n)}$ are normalized by requiring $C_n(0) = 1$. This implies that $\langle 0|O_n|m\rangle \approx \delta_{mn}$ if the states are normalized as $\langle m|n\rangle = \delta_{mn}$.

Although the operator basis in each channel is large, it is found that the correlation function of the operator O_1 optimized for the ground state still has a sizeable contribution from other states; namely, the effective mass function does not show a good enough plateau in the early time range (especially in the E^{++} channel), as shown in Fig. 3. In order to enhance the contribution of the ground state to the corresponding correlation functions, we construct another type of gluonic operator in terms of the gauge potential $A_\mu(x)$ [10, 11] in the Coulomb gauge.

B. Glueball operators in terms of $A_\mu(x)$

According to the definition of the gauge link oriented in the μ direction starting from the lattice site, *i.e.*, $U_\mu(x) = \exp[-iagA_\mu(x)]$, up to an irrelevant pre-factor, we have

$$A_\mu(x) \equiv i \ln U_\mu(x) \quad (6)$$

where $\ln U_\mu(x)$ can be derived as $\ln U_\mu(x) = V(x) \text{diag}(\ln \lambda_1(x), \ln \lambda_2(x), \ln \lambda_3(x)) V^\dagger(x)$ with $\lambda_{1,2,3}(x)$ being the ei-

genvalues of $U_\mu(x)$ and $V(x)$ being the unitary matrix that diagonalizes $U_\mu(x)$. The properties of $U_\mu(x) \in SU(3)$ require $\lambda_1 \cdot \lambda_2 \cdot \lambda_3 = 1$ and $|\lambda_{1,2,3}| = 1$, such that $\lambda_{1,2,3}$ can be expressed as $\lambda_i = e^{i\theta_i}$ ($i = 1, 2, 3$) with $\theta_i \in [-\pi, \pi]$.

On each time slice, the spatially extended operator $O_A^R(r, t)$ can be constructed by $A_\mu(x)$ at two different points. For $P = C = +$, the explicit expression of $O_A^R(r, t)$ of the quantum number R^{PC} is

$$O_A^R(\mathbf{x}, t; r) = \frac{1}{N_r} \sum_{ij, |\mathbf{r}|=r} \text{tr} S_{ij}^R [A_i(\mathbf{x} + \mathbf{r}) A_j(\mathbf{x})], \quad (7)$$

where N_r is the degeneracy of \mathbf{r} with the same r and S_{ij}^R are the combinational coefficients related to the irrep R of the spatial symmetry group O (octahedral group) on the lattice. For $R = A_1, E, T_2$, the non-zero values of S_{ij}^R are as follows:

$$\begin{aligned} S_{11}^{A_1} &= S_{22}^{A_1} = S_{33}^{A_1} = 1 \\ S_{11}^{E,1} &= -S_{22}^{E,1} = \frac{1}{\sqrt{2}} \\ S_{11}^{E,2} &= S_{22}^{E,2} = -\frac{1}{\sqrt{6}}, \quad S_{33}^{E,2} = \frac{2}{\sqrt{6}} \\ S_{jk}^{T_2,i} &= |\epsilon_{ijk}|, \quad i, j, k = 1, 2, 3. \end{aligned} \quad (8)$$

The $O_A^R(r, t)$ operator for A_1^{+-} is defined as

$$O_A^{A_1^{+-}}(\mathbf{x}, t; r) = \frac{1}{N_r} \sum_{|\mathbf{r}|=r} \epsilon_{ijk} \text{tr} [A_i(\mathbf{x} + \mathbf{r}) A_j(\mathbf{x})] \hat{r}_k, \quad (9)$$

where $\hat{\mathbf{r}}$ is the orientation vector of \mathbf{r} .

In each channel, through the implementation of CDER similar to Eqs. (2) and (3) and using the same $r_c = 7a$, we calculate the correlation function $C_{An}(r, t)$ of O_A^R and the n -th optimized operator O_n :

$$\begin{aligned} C_{An}(r, t) &= \frac{1}{T} \sum_{\tau, \mathbf{x}, \mathbf{y}} \langle 0|O_A^R(\mathbf{x}, t + \tau; r) O_n(\mathbf{y}, \tau)|0\rangle \\ &\approx \Phi_n(r) e^{-m_n t} + \sum_{i \neq n} \epsilon_m \Phi_m(r) e^{-m_i t}, \end{aligned} \quad (10)$$

where the last parametrization is due to predominant coupling of O_n to the n -th state with $\epsilon_i \ll 1$, and $\Phi_n(r) \propto \langle 0|O_A^R(\mathbf{0}, t; r)|n\rangle$ is interpreted as the Bethe-Salpeter (BS) wave function [12] of the n -th state $|n\rangle$ if it is a two-gluon glueball state. In principle, $\Phi_n(r)$ can be approximated by $C_{An}(r, t)$ at any t according to Eq. (10). However, owing to the rapid increase in the noise, we can only observe clear signals of $\Phi_n(r)$ at the first few time slices. Figure 4 shows the profiles of $\Phi_{1,2}(r)$ at $t = 0$ for A_1^{++} , A_1^{+-} , E^{++} , and T_2^{++} channels on 48I and 64I lattices

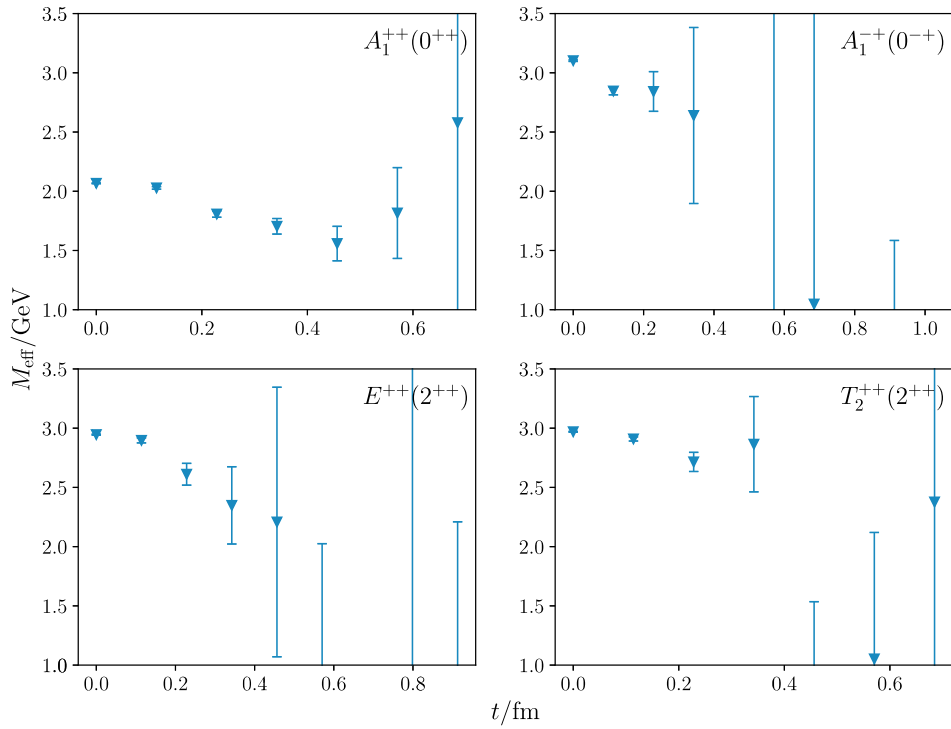


Fig. 3. (color online) The effective mass plots of the correlation functions $C_1(t)$ in Eq. (5) for A_1^{++} , E^{++} , T_2^{++} , and A_1^{-+} channels on 48l.

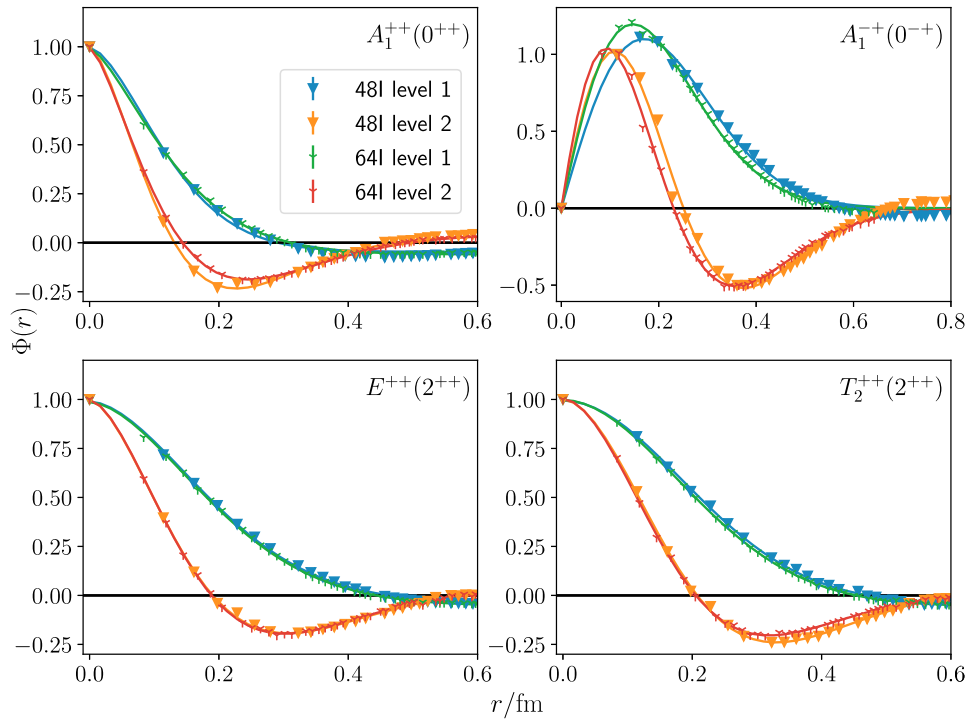


Fig. 4. (color online) Normalized BS wave functions of the ground and first excited states on the 48l and 64l lattices.

(normalized by $\Phi(r=0) = 1$ for $PC = ++$ channels and $\Phi(r=a) = 1$ for the A_1^{-+} channel), where the values of r are converted into physical units using the lattice spacings a in Table 1. Similar to that in Refs. [10, 11], the

data points of $\Phi_n(r)$ can be described by some phenomenological functional forms. For the ground state and first excited state of A_1^{++} , E^{++} , and T_2^{++} , the functions take the forms

$$\begin{aligned}\Phi_1(r) &= Ae^{-(r/r_0)^\alpha} + D \\ \Phi_2(r) &= A(1 - \beta r^\alpha)e^{-(r/r_0)^\alpha} + D'.\end{aligned}\quad (11)$$

For A_1^{-+} , the corresponding function forms are

$$\begin{aligned}\Phi_1(r) &= Are^{-(r/r_0)^\alpha} + D \\ \Phi_2(r) &= Ar(1 - \beta r^\alpha)e^{-(r/r_0)^\alpha} + D'.\end{aligned}\quad (12)$$

In the functions forms above, the constants D and D' are added to account for the possible contamination from the unphysical modes of domain-wall sea quarks, as will be explained in a later section. By using these functions forms to fit $C_{An}(r, t=0)$ in each channel, we obtain the parameters α, β, r_0 , whose best-fit values are given in Table 2. These functions with the fitted parameters are also plotted in Fig. 4 as curves. It is seen that the functions describe the data points fairly well. It is interesting that the r -behaviors of $\Phi_{1,2}(r)$ in $PC = ++$ channels are very similar to the radial $1S$ and $2S$ Schrödinger wave function of a two-body system with a central potential. These behaviors and the parameters α and r_0 are very similar to those obtained in the quenched approximation [11]. The BS wave functions in the A_1^{-+} channel are derived for the first time on the lattice and have the feature of $1P$ and $2P$ wave functions. Note that, by solving the Bethe-Salpeter equation of the 0^{-+} glueball, the two-body P -wave feature of the 0^{-+} Bethe-Salpeter amplitude was

also observed in Refs. [13–15].

We would not like to put too much emphasis on the interpretation of the wave functions $\Phi_n(r)$ but will use the feature of the r -behaviors of these functions to enhance the contribution of the ground states in the early time region. Because $\Phi_2(r)$ in each channel has a radial node at $r = r_1$, the correlation function $C_{A1}(r_1, t)$ in each channel is expected to be dominated by the ground state, as the second term in Eq. (10) is further suppressed by $\Phi_2(r_1) \approx 0$. According to Fig. 4, the radial node of $\Phi_2(r)$ appears at $r \sim 0.12, 0.19$ and 0.22 fm in the scalar (A_1^{++}), the tensor (E^{++} and T_2^{++}), and the pseudoscalar channel (A_1^{-+}), respectively. According to the lattice spacings in Table 1, we choose $r_1(A_1^{++})/a = \sqrt{2}$, $r_1(E^{++}, T_2^{++})/a = \sqrt{3}$, and $r_1(A_1^{-+})/a = 2$ on the 48I lattice. On the 64I lattice, these r_1/a 's are chosen to be $\sqrt{5}$, $\sqrt{5}$, and $2\sqrt{2}$. At these values of r_1 , the $\Phi_2(r)$ values are seen to be approximately zero. The effective mass of each $C_{An}(r_1, t)$ for all four channels on the two ensembles (48I and 64I) are illustrated in Fig. 5, where the vertical axis and the horizontal axis are plotted in physical units. It is seen that the effective masses show more or less plateaus at the first several time slices, which indicates that $C_{A1}(r_1, t)$ can be described with a single exponential, as expected.

With the prescription mentioned above, the ground state masses in each channel are extracted through single exponential function forms in early time windows. In each panel of Fig. 5, the grey bands illustrate the fitting results and the time intervals of the fits. In order to exhibit the efficacy of the CDER method, we also show the lattice data that are derived by calculating the correlation functions without the implementation of CDER in green (48I ensemble) and yellow bands (64I ensemble). Obviously, the data without CDER fluctuate drastically with respect to time, and the errors are quite large. In contrast, the data points based on the CDER method have much smaller errors at the first 4-6 time slices and show more or less plateaus. From the plateau regions indicated by the grey bands in Fig. 5, we obtain estimates of the ground state mass values, which are listed in Table 3 in physical units. We make the following observations:

- Given the small errors at the first several time slices, the data points do not behave very regularly but fluctuate slightly. For each channel, the effective masses from both ensembles are very close at $t = 0$ but become more different when t increases. A possible reason for this behavior is the contamination of oscillatory modes of the domain wall sea quarks (see below). Anyway, given the large errors, the fitted ground state masses on the 48I and 64I ensembles are compatible with each other except for the A_1^{++} channel.

- The masses of ground states in E^{++} and T_2^{++} channels are compatible with each other on the same en-

Table 2. Fitted parameters of Bethe-Salpeter wave function form in Eqs. (11) and (12).

	R^{PC}	n	r_0 /fm	α	β
48I	A_1^{++}	1	0.14(4)	1.6(2)	
		2	0.16(5)	1.5(2)	24(1)
	E^{++}	1	0.24(7)	1.8(2)	
		2	0.22(5)	1.6(2)	16(1)
	T_2^{++}	1	0.26(9)	2.0(3)	
		2	0.25(8)	1.8(3)	19(2)
	A_1^{-+}	1	0.24(8)	1.9(3)	
		2	0.23(7)	1.8(3)	12(1)
64I	A_1^{++}	1	0.15(3)	1.4(1)	
		2	0.20(10)	1.5(4)	18(2)
	E^{++}	1	0.24(6)	1.7(2)	
		2	0.22(8)	1.7(3)	17(2)
	T_2^{++}	1	0.26(6)	1.9(2)	
		2	0.23(5)	1.8(2)	18(1)
	A_1^{-+}	1	0.20(5)	1.7(2)	
		2	0.19(6)	1.6(2)	10(1)

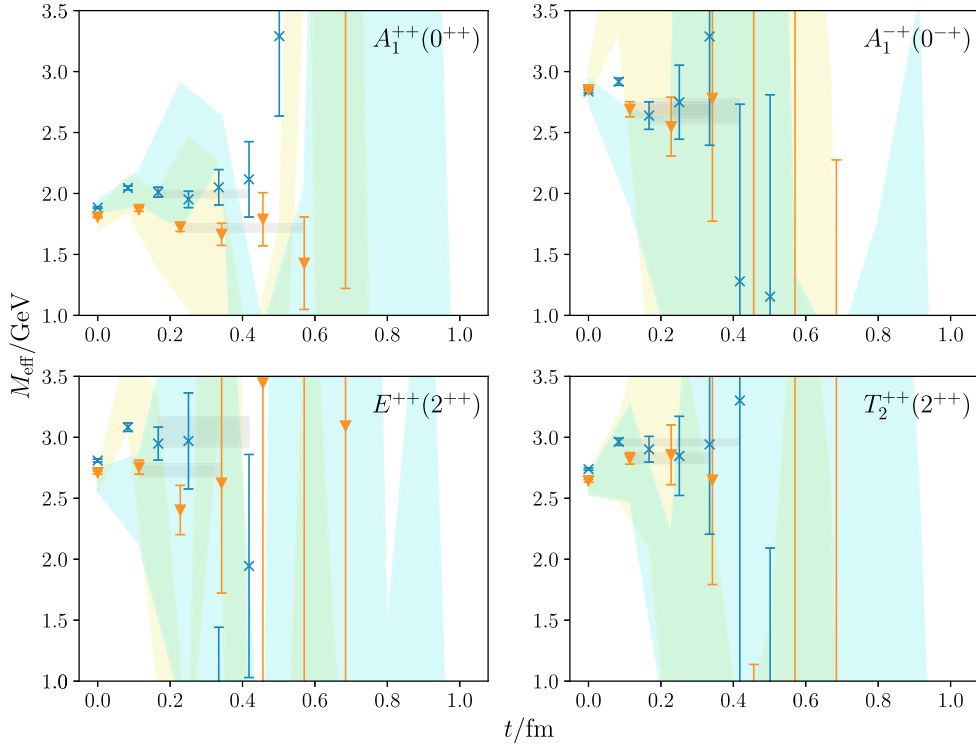


Fig. 5. (color online) Effective masses of $C_{A1}(r_1, t)$ on 48I (orange triangles) and 64I (blue crosses), with the shaded region showing the results obtained without CDER. The gray bands show the fitting results and fitting windows obtained through single-exponential function forms.

Table 3. Fitted masses of the ground states in $A_1^{++}, E^{++}, T_2^{++}, A_1^{-+}$ channels on 48I and 64I ensembles. The masses are converted into values in physical units (GeV) using the lattice spacings in Table 1.

ensemble	$m(A_1^{++})$	$m(E^{++})$	$m(T_2^{++})$	$m(A_1^{-+})$
48I	1.718(34)	2.729(54)	2.829(46)	2.685(60)
χ^2/dof	0.76	0.82	0.01	0.12
64I	1.995(30)	3.05(13)	2.958(28)	2.67(10)
χ^2/dof	0.18	1.95	0.09	0.22

semble. This also indicates that the discretization effects are not important, because these states correspond to the 2^{++} state in the continuum limit.

- Their masses are higher than but not far from those of the quenched approximation predictions and preliminary full-QCD calculations [1–5].

The fluctuating data points of the effective masses and the constant terms in (11) and (12) may be attributed to the contamination of unphysical oscillatory modes of the domain wall fermions [16–18]. In the mean field approximation, the lowest unphysical mode of domain wall fermions propagates along time as $e^{-Et} \sim (-)^{t/a} e^{-|E_0|t}$, with E_0 being expressed as

$$E_0 = \frac{1}{a} \ln \left| \frac{4 - M_5 - 3u_0}{u_0} \right|, \quad (13)$$

where M_5 is the domain-wall mass parameter and u_0 is the tadpole parameter of gauge links. These modes may contribute to correlation functions of gluonic operators through the vacuum polarization of a pair of (physical and unphysical) a quark and antiquark. According to the discussion in the reference mentioned above, the energy of the unphysical fermion mode is estimated as $|E_0|a \sim 0.716$ for the 48I ensemble ($M_5 = 1.8$, $u_0 = 0.876$) and $|E_0|a \sim 0.660$ for the 64I ensemble ($M_5 = 1.8$, $u_0 = 0.886$). Using the lattice spacing $a^{-1} \approx 1.734$ GeV for 48I and $a^{-1} \approx 2.360$ GeV for 64I, the lowest energy of the excitation of a physical quark and an unphysical quark from the vacuum can be as low as roughly $m_2 \sim 1.24$ GeV for 48I and 1.56 GeV for 64I, respectively, both of which are lower than the expected 0^{++} glueball mass and worrisome in the data analysis of the correlation functions of gluonic operators.

As indicated by the BS amplitudes shown in Fig. 4, the contributions from glueball states are expected to be highly suppressed in comparison with the $r=0$ case. Thus, we check the effective mass of $C_{n1}(r, t)$ at a large r in the A_1^{++} channel, to enhance the contribution from the oscillatory modes. Figure 6 shows the effective masses of $C_{A1}(r, t)$ in the $A_1^{++}(0^{++})$ channel at $r \approx 0.6$ fm (where the

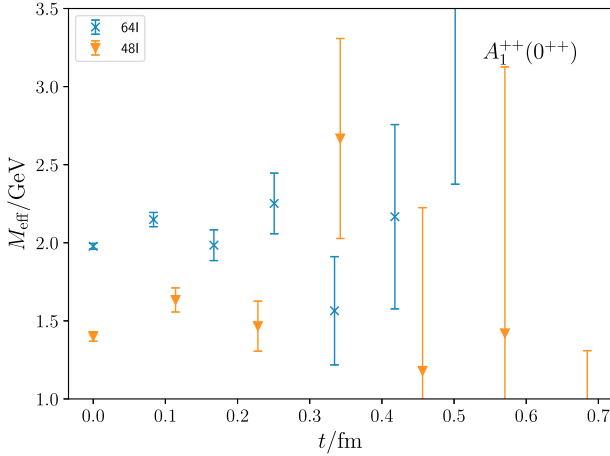


Fig. 6. (color online) Effective masses of $C_{A_1}(0.6 \text{ fm}, t)$ on 48I (orange triangles) and 64I (blue crosses), where the glueball contribution is suppressed and then the oscillatory behavior is more obvious than that in Fig. 5.

glueball contribution is expected to be roughly 10 times smaller than that at $r = 0$ according to the BS wave function). Here, the orange and blue points refer to those from the 48I and 64I ensembles, respectively. At the early time slices, the data points oscillate up and down. The magnitude increases with time and can be understood through the following expression:

$$\begin{aligned}
 m_{\text{eff}}(t) &= \frac{1}{a} \ln \frac{C(t)}{C(t+a)} \\
 &= m_1 + \frac{1}{a} \ln \frac{1 + (-)^{t/a} B e^{-\Delta t}}{1 + (-)^{t/a+1} B e^{-\Delta(t+a)}} \\
 &\xrightarrow{|B| \ll 1} m_1 + \frac{B}{a} (1 + e^{-\Delta a}) (-)^{t/a} e^{-\Delta t}, \quad (14)
 \end{aligned}$$

where the correlation function $C(t) = A e^{-m_1 t} (1 + (-)^{t/a} B e^{-\Delta t})$ includes both the physical states (glueballs, first term) and the oscillatory modes (second term). On the 48I and 64I ensembles we used, the mass of the oscillatory modes can be even lower than the glueball mass around 1.7–2.0 GeV, which leads to $\Delta < 0$. Then, $e^{-\Delta t}$ increases on t ; and the effect on 64I should be weaker than that on 48I. Such a prediction is consistent with the observation in Fig. 6, as the oscillation seems to be stronger at a larger t and/or lattice spacing (orange points of 48I at $a = 0.11 \text{ fm}$ v.s. blue points of 64I at $a = 0.08 \text{ fm}$).

The situation for glueballs is even more complicated in the presence of dynamical quarks. Experimentally, most of hadrons are observed as resonances; therefore, their decays should be taken into account. The energy levels obtained on the lattice are actually the eigen energies of the lattice Hamiltonian, and their connection with the resonances in the real world is highly nontrivial. In full QCD, glueballs can mix with $\bar{q}q$ and multi-hadron states. However, with the gluonic operators, the $\bar{q}q$ states

are suppressed by $O(1/N_c)$ and two meson states are suppressed by $O(1/N_c^2)$. This is perhaps the reason why we see the effective mass plateaus in short time separation. To have a complete picture, it is essential to include quark operators in the calculation, which is beyond the scope of the present work. There is an exploratory lattice study in this direction in the scalar channel [19], but no glueball states can be identifiable unambiguously yet. In this sense, our work makes a little progress in this direction.

III. SUMMARY

An exploratory study of glueballs is performed on two $N_f = 2 + 1$ gauge ensembles with large lattice sizes and the dynamical quark masses being tuned at the physical point. The large lattice size enables us to use the CDER technique to reduce the errors of the correlation functions of glueball operators. By using the spatially extended glueball operators defined through the gauge potential $A_\mu(x)$ in the Coulomb gauge, the Bethe-Salpeter wave functions of the scalar (A_1^{++}), the tensor ($E_2^{++} \oplus T_2^{++}$), and the pseudoscalar (A_1^{-+}) states are derived, which are similar to the features of the non-relativistic wave functions of two-body systems. Even though the physical meaning of these BS wave functions may not be clear, we can make use of their radial behaviors to further improve the ground state domination of the related correlation functions at the early time region, where the ground state masses in each channel can be extracted through single-exponential function form. If the excited state contamination is small and the couplings to $\bar{q}q$ meson states are negligible (they can show up at very large time separation given enough statistics), the ground state masses we obtained in the scalar, tensor, and pseudoscalar channels are not far from the corresponding glueball masses in the quenched approximation. In addition to the uncontrolled systematic uncertainties due to the possible mixing with $q\bar{q}$ states and multi-hadron states, our results may suffer from the interference from the unphysical modes of domain wall fermions. A scrutinized full-QCD study should be carried out in which the $\bar{q}q$ and multi-meson operators are included and the resonance nature of most hadrons is considered. As a noise reduction scheme, the same CDER technique can be applied to all the correlation functions involving the disconnected quark insertions. In this sense, our study represents a breakthrough for improving the signal-to-noise ratios of correlation functions involving glueball operators and paves the way to the final answer on the existence of the glueball states.

ACKNOWLEDGEMENTS

We thank the RBC and UKQCD collaborations for providing us their DWF gauge configurations.

References

- [1] C. J. Morningstar and M. J. Peardon, *Phys. Rev. D* **60**, 034509 (1999), arXiv:hep-lat/9901004
- [2] Y. Chen *et al.*, *Phys. Rev. D* **73**, 014516 (2006), arXiv:hep-lat/0510074
- [3] C. M. Richards, A. C. Irving, E. B. Gregory *et al.* (UKQCD Collaboration), *Phys. Rev. D* **82**, 034501 (2010), arXiv:1005.2473[hep-lat]
- [4] E. Gregory, A. Irving, B. Lucini *et al.*, *JHEP* **10**, 170 (2012), arXiv:1208.1858[hep-lat]
- [5] W. Sun, L.-C. Gui, Y. Chen *et al.*, *Chin. Phys. C* **42**, 093103 (2018), arXiv:1702.08174[hep-lat]
- [6] W. Sun, A. Alexandru, Y. Chen *et al.* (χ QCD Collaboration), *Chin. Phys. C* **42**, 063102 (2018), arXiv:1507.02541[hep-ph]
- [7] K.-F. Liu, J. Liang, and Y.-B. Yang, *Phys. Rev. D* **97**, 034507 (2018), arXiv:1705.06358[hep-lat]
- [8] Y.-B. Yang, M. Gong, J. Liang *et al.*, *Phys. Rev. D* **98**, 074506 (2018), arXiv:1805.00531[hep-lat]
- [9] T. Blum *et al.* (RBC, UKQCD Collaboration), *Phys. Rev. D* **93**, 074505 (2016), arXiv:1411.7017[hep-lat]
- [10] P. de Forcrand and K.-F. Liu, *Phys. Rev. Lett.* **69**, 245 (1992)
- [11] J. Liang, Y. Chen, W.-F. Chiu *et al.*, *Phys. Rev. D* **91**, 054513 (2015), arXiv:1411.1083[hep-lat]
- [12] E. E. Salpeter and H. A. Bethe, *Phys. Rev.* **84**, 1232 (1951)
- [13] E. V. Souza, M. Narciso Ferreira, A. C. Aguilar *et al.*, *Eur. Phys. J. A* **56**, 25 (2020), arXiv:1909.05875[nucl-th]
- [14] M. Q. Huber, C. S. Fischer, and H. SanchisAlepez, *The European Physical Journal C* **80** (2020)
- [15] M. Q. Huber, C. S. Fischer, and H. Sanchis-Alepuz, *Eur. Phys. J. C* **81**, 1083 (2021)
- [16] J. Liang, Y. Chen, M. Gong *et al.*, *Phys. Rev. D* **89**, 094507 (2014), arXiv:1310.3532[hep-lat]
- [17] R. S. Sufian, M. J. Glatzmaier, and Y.-B. Yang, arXiv:1603.01591
- [18] M. Tomii, *Phys. Rev. D* **96**, 074504 (2017), arXiv:1706.03099[hep-lat]
- [19] R. Brett, J. Bulava, D. Darvish *et al.*, *AIP Conf. Proc.* **2249**, 030032 (2020), arXiv:1909.07306[hep-lat]